Journal of Biomedical Optics

BiomedicalOptics.SPIEDigitalLibrary.org

# Dry coupling for whole-body small-animal photoacoustic computed tomography

Chenghung Yeh
Lei Li
Liren Zhu
Jun Xia
Chiye Li
Wanyi Chen
Alejandro Garcia-Uribe
Konstantin I. Maslov
Lihong V. Wang

SPIE.

Chenghung Yeh, Lei Li, Liren Zhu, Jun Xia, Chiye Li, Wanyi Chen, Alejandro Garcia-Uribe, Konstantin I. Maslov, Lihong V. Wang, "Dry coupling for whole-body small-animal photoacoustic computed tomography," *J. Biomed. Opt.* **22**(4), 041017 (2017), doi: 10.1117/1.JBO.22.4.041017.

Journal of Biomedical Optics 22(4), 041017 (April 2017)

# Dry coupling for whole-body small-animal photoacoustic computed tomography

**Chenghung Yeh,[a,†] Lei Li,[a,†] Liren Zhu,[b] Jun Xia,[c] Chiye Li,[b] Wanyi Chen,[b] Alejandro Garcia-Uribe,[b] Konstantin I. Maslov,[b] and Lihong V. Wang[a,b,*,‡]**
[a]Washington University, Department of Electrical and Systems Engineering, St. Louis, Missouri, United States
[b]Washington University, Department of Biomedical Engineering, St. Louis, Missouri, United States
[c]University at Buffalo, Department of Biomedical Engineering, Buffalo, New York, United States

**Abstract.** We have enhanced photoacoustic computed tomography with dry acoustic coupling that eliminates water immersion anxiety and wrinkling of the animal and facilitates incorporating complementary modalities and procedures. The dry acoustic coupler is made of a tubular elastic membrane enclosed by a closed transparent water tank. The tubular membrane ensures water-free contact with the animal, and the closed water tank allows pressurization for animal stabilization. The dry coupler was tested using a whole-body small-animal ring-shaped photoacoustic computed tomography system. Dry coupling was found to provide image quality comparable to that of conventional water coupling.  [DOI: 10.1117/1.JBO.22.4.041017]

Keywords: dry coupling; water immersion; whole-body small-animal imaging; photoacoustic computed tomography.

Paper 160544SSR received Aug. 10, 2016; accepted for publication Feb. 8, 2017; published online Feb. 23, 2017.

Whole-body small-animal imaging is widely used in biomedical research for studying and modeling human disease.[1] However, most whole-body small-animal imaging modalities, such as magnetic resonance imaging (MRI),[2] positron emission tomography (PET),[3] and x-ray computed tomography (CT),[4] have limitations. For example, MRI requires an expensive high magnetic field and long imaging time, and x-ray CT and PET utilize ionizing radiation, which may confound longitudinal experimental results.[5–7]

Recently, there has been increased interest in whole-body small-animal photoacoustic tomography (PAT). In PAT, photons are absorbed by biomolecules in tissue, and subsequently the converted heat produces ultrasonic pressure waves via thermoelastic expansion.[8] By detecting these pressure waves, PAT yields high-resolution images in both the ballistic and diffusive optical regimes.[9,10] Over the past few years, multiple whole-body small-animal PAT systems have been implemented using different acoustic coupling media, light delivery systems, and acoustic detection designs.[11–16] However, due to their limited detection views, linear array photoacoustic CT,[17] hemispherical array photoacoustic CT,[18] and half-ring multispectral optoacoustic tomography (MSOT)[13] generally require rotating the animal to achieve full view detection. Moreover, MSOT with fiber bundles illumination lacks uniformity in light delivery, which affects image quality. In 2011, we introduced ring-shaped confocal photoacoustic CT (RC-PACT),[14] which utilizes full-ring light illumination and full-ring acoustic detection to address these issues. However, similar to other whole-body small-animal imaging systems, RC-PACT still uses water as a direct-contact coupling medium, which can induce anxiety[19,20] and water-immersion wrinkling in mice.[21] Both of these factors can render physiological measurements inaccurate in various ways, such as by decreasing T-cell blastogenesis,[19] altering blood flow velocity,[21] and inducing vasoconstriction.[21] Here, we report a ring-shaped dry-coupled confocal photoacoustic CT system (RDC-PACT) that overcomes these limitations. RDC-PACT uses a tubular elastic latex membrane animal holder to achieve dry coupling and employs free-space full-ring light delivery to provide high fluence and uniform illumination. As shown in Fig. 1(a), the system uses a solid-state laser (DLS 9050, Continuum) with a 7-ns pulse duration and 50-Hz pulse repetition rate. The laser beam passes through a conical lens (cone angle 130 deg, Delmar Photonics) to form a ring-shaped light beam and is homogenized by an optical diffuser (EDC-5, RPC Photonics). The beam is focused by a homemade acrylic condenser to achieve full-ring light delivery. The maximum light intensity at the surface of the animal is $\sim 20\ \mathrm{mJ/cm^2}$ at 1064 nm (The pulse energy we used for *in vivo* experiments was 70 mJ, the width of the mouse trunk is ~22 mm, and the height of the ring beam on skin is ~5 mm. Assuming that the mouse trunk was a cylinder shape, we then estimated that the surface fluence was $\sim 20\ \mathrm{mJ/cm^2}$), which is below the safety limit set by the American National Standards Institute (ANSI).[22] The generated photoacoustic waves are detected by a custom-made 512-element full-ring ultrasonic transducer array with a 5-MHz central frequency (>84% one-way detection bandwidth, Imasonic SAS). Each element has a cylindrical focus (0.2 NA, 20-mm element elevation size, 0.61-mm pitch, and 0.1-mm interelement spacing). Compared to the existing RC-PACT system,[14] the RDC-PACT system employs a larger full-ring ultrasonic transducer array (10 versus 5 cm in diameter), which can accommodate larger animals. The system provides ~0.1-mm in-plane resolution and ~1-mm elevational resolution. Raw channel data from each element are digitized in parallel using a 512-channel data acquisition system (four SonixDAQs, Ultrasonix Medical ULC, each 128 channels,

*Address all correspondence to: Lihong V. Wang, E-mail: lvw@caltech.edu

†These authors contributed equally.

‡L.V.W. is now Bren Professor of Medical Engineering and Electrical Engineering at California Institute of Technology, Pasadena, California.

1083-3668/2017/$25.00 © 2017 SPIE

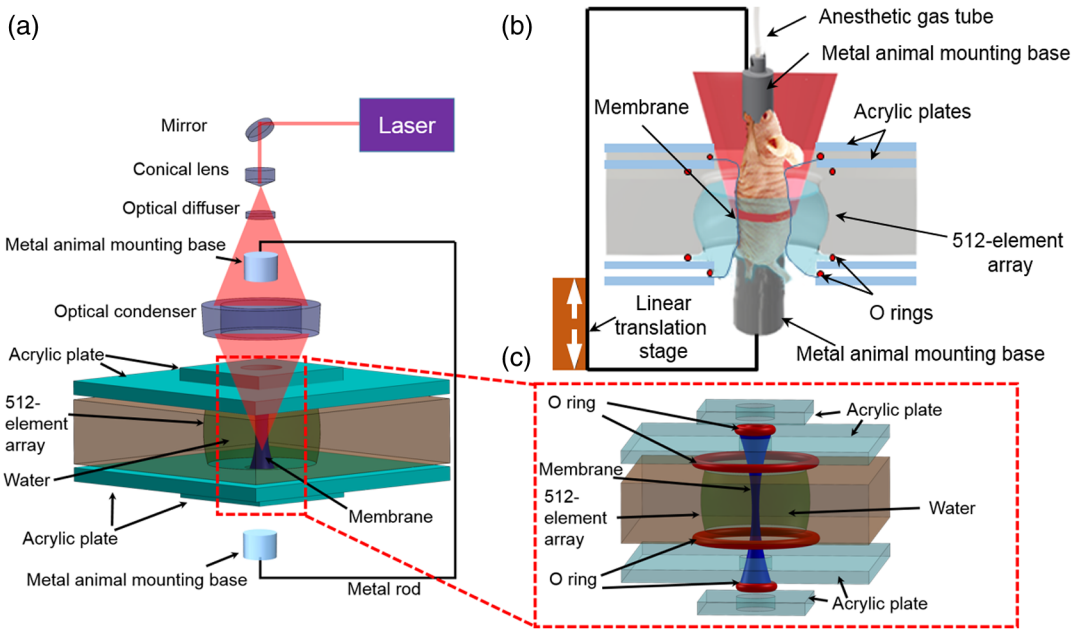


**Fig. 1** (a) Schematic diagram of the full-ring dry-coupled confocal whole-body photoacoustic CT (RDC-PACT) system. (b) Setup of the animal holder. (c) Setup of the dry coupling device.

40-MHz sampling rate, and 12-bit dynamic range). Images are reconstructed using the universal backprojection algorithm.[14]

A detailed view of the animal holder is shown in Fig. 1(b). The upper and lower animal mounting bases are aluminum tubes, and the upper base is connected to the anesthesia gas supply tube. The aluminum tubes are fastened to fixed metal rods (Mini-series mounting post, Thorlabs) and moved by a one-dimensional stage (LP28, Parker). The animal is secured by taping its fore and hind legs to the aluminum tubes. Ultrasound gel is then applied to the animal's skin. The rigid design of the metal rods and aluminum tubes minimizes holder movement caused by animal motion such as respiration. A detailed view of the membrane and water tank is shown in Fig. 1(c). The water is confined by four O rings and the tubular membrane, and the animal is placed upright inside the membrane tube, which prevents direct water contact. Moreover, the thin membrane (~20 $\mu$m in thickness) minimizes light and sound attenuation. The gel layer potentially contains bubbles, which distort and reflect ultrasound signal, causing reconstruction artifacts. To mitigate these, the closed water tank design allows pressurization that minimizes the gap between the mouse skin and membrane, achieving the best possible coupling. The water pressurization also stabilizes the imaging region without stressing the entire animal by using fiber glass rods or thin wires in tension, as employed in previous whole-body small-animal imaging systems.[14] Moreover, the dry coupling system can potentially be rotated 90 deg and the animal mounted horizontally, similar to a CT or MRI scanner. The animal can be laid on an imaging bed that can be quickly slid in and out. The closed water tank also avoids contamination from animal waste during experiments, simplifying system maintenance.[14] Moreover, the system can also be easily switched to water coupling by removing the membrane [Fig. 1(c)] and sealing the bottom with a flexible membrane.

To experimentally compare traditional water coupling and dry coupling in RDC-PACT, we imaged a healthy mouse (Hsd: Athymic Nude-Foxnl$^{NU}$, Harlan). All the experimental procedures were carried out in conformity with laboratory animal protocols approved by the Animal Studies Committee at Washington University in St. Louis. Throughout the experiment, the mouse was maintained under anesthesia with 1.5% vaporized isoflurane. The same excitation, acquisition, and reconstruction settings were applied to both water coupling and dry coupling experiments. Water-coupled images are shown in Figs. 2(a) and 3(a). Dry-coupled images are shown in Figs. 2(b) and 3(b). Both water-coupled and dry-coupled images were acquired at 1064 nm, where endogenous hemoglobin is the main contrast. All the images clearly show the liver, spleen, and kidneys. Moreover, the entire vascular structure within the organs is visible, including the renal artery and venous loop. Further, the spinal cord, backbone muscle, gastrointestinal (GI) tract, superior mesentery vein, and vena cava are clear.

We have experimentally measured the in-plane resolution by imaging tungsten wires (30 $\mu$m in diameter). The quantified resolution is 125 $\mu$m, as shown in Fig. 2. Next, we examined whether dry coupling could achieve the same image quality as traditional water coupling. To better compare the image quality, we plotted the contrast-to-noise ratio (CNR) from several features in the liver region [Figs. 3(a) and 3(b)], with close-ups highlighting one typical feature. Remarkably, both water coupling and dry coupling had similar CNRs (28.8 and 30.4, respectively) in the overall liver region [Fig. 3(c)]. The CNR was calculated as the peak-to-peak PA amplitude in the region of interest (ROI), divided by two times the standard deviation of the background amplitude, where the ROIs are labeled by the red and blue squares in Figs. 3(a) and 3(b). Next, we compared the kidney region (Fig. 4), where more organs can be imaged. The CNR values here (dry coupling, 11.0; water coupling, 10.3) show that dry coupling can maintain the image quality. The comparable CNRs indicate that dry coupling can successfully remove bubbles in the gel layer by pressurization.

To demonstrate the capability of continuous whole-body small-animal dry-coupled scanning, we imaged a mouse over a 26-mm length, from the kidney to the heart region. A series of *in vivo* images is shown in Video 1. For comparison, the same images were also acquired in water coupling and are shown in

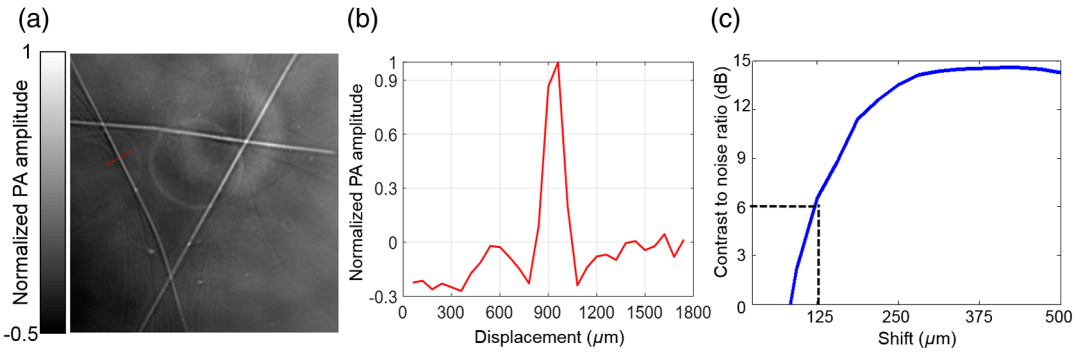


**Fig. 2** In-plane resolution quantification. (a) PA image of three crosswise tungsten wires. (b) The photoacoustic amplitude distribution along the red line in (a). (c) The CNR versus the shift in the sum of the original line profile shown in (b) and the shifted one. The in-plane resolution, defined as the shift corresponding to 6-dB CNR, is 125 $\mu$m.

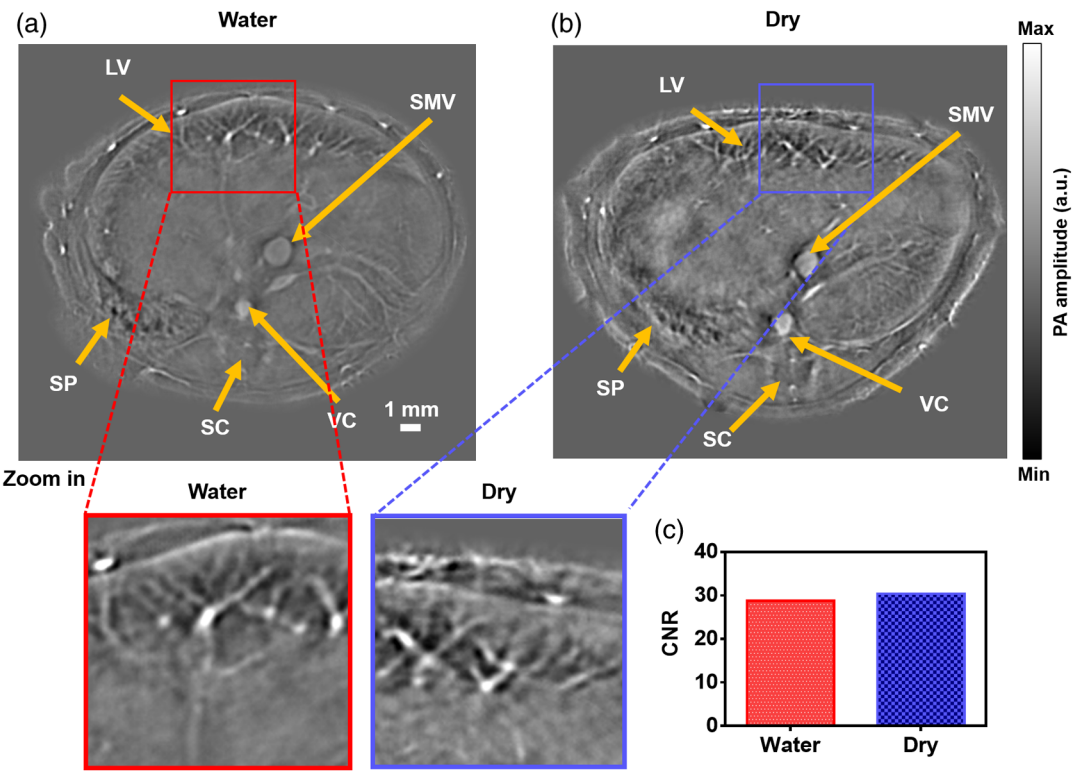


**Fig. 3** Comparative *in vivo* RC-PACT imaging of the liver region of a nude mouse. (a) Water coupling and (b) dry coupling images of a nude mouse at the liver region. Detailed view of the red box in the water coupling image and detailed view of the blue box in dry coupling image. (c) CNR of the water coupling and dry coupling images. LV, liver; SC, spinal cord; SMV, superior mesentery vein; SP, spleen; VC, vena cava. (Video 1, MP4, 5.35 MB [URL: http://dx.doi.org/10.1117/1.JBO.22.4.041017.1]).

Video 2. When pressurization was applied, dry-coupled scanning caused less movement during elevational scanning.

In comparison with earlier whole-body small-animal PAT systems, the specific design of the water tank eliminates water-induced stress and wrinkling. Moreover, our RDC-PACT, based on confocal full-ring light delivery, enables fast full-view cross sectional imaging. In contrast, half-ring,[12] and hemispherical array[18] based PAT systems have limited detection views and associated image reconstruction artifacts. In addition, the half-ring-based system envelops the whole mouse in membrane,[13] while in our system only the region being imaged is in contact with the membrane and coupling gel. Therefore, our system facilitates access to the animal's lower body by additional sensors, such as lead II and lead III of an ECG[23,24] to monitor the heart rate and impedance pneumography leads to measure respiration. Because most of the body regions are accessible in our system, we can also easily perform intraperitoneal injection or vein injection at the mouse's fore and hind paws and tail.

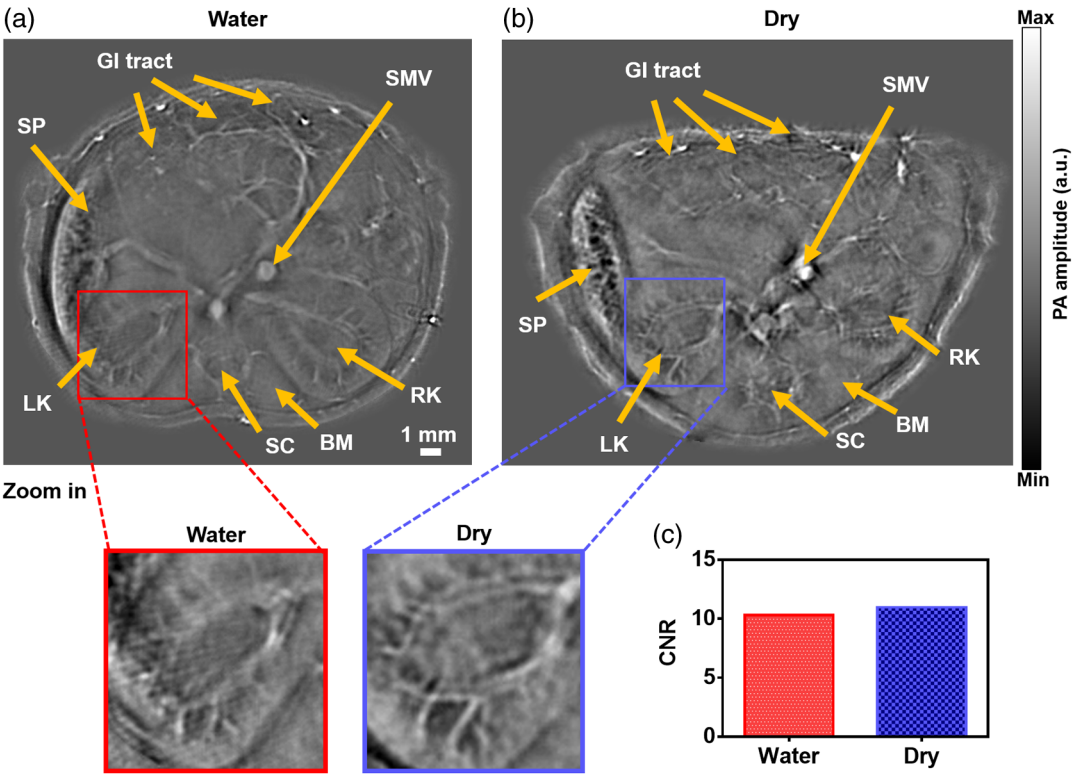


**Fig. 4** Comparative *in vivo* RC-PACT imaging of the kidney region of a nude mouse. (a) Water coupling and (b) dry coupling images of a nude mouse at the kidney region. Detailed view of the red box in the water coupling image and detailed view of the blue box in the dry coupling image. (c) CNR of the water coupling and dry coupling images. BM, backbone muscle; GI, GI tract; LK, left kidney; RK, right kidney; SC, spinal cord; SMV, superior mesentery vein; SP, spleen. (Video 2, MP4, 1.99 MB [URL: http://dx.doi.org/10.1117/1.JBO.22.4.041017.2]).

## *Disclosures*

L.V.W. has financial interests in Microphotoacoustics, Inc. and Endra, Inc., neither of which supported this work. K. Maslov has a financial interest in Microphotoacoustics, Inc.

## *Acknowledgments*

The authors appreciate the close reading of the manuscript by Prof. James Ballard. We also thank Chin Ting, Junjie Yao, Jinyang Liang, and Yong Zhou for helpful discussions. This work was sponsored by the National Institutes of Health Grants DP1 EB016986 (NIH Director's Pioneer Award), R01 CA186567 (NIH Director's Transformative Research Award), and R01 EB016963.

## *References*

1. F. Kiessling, B. J. Pichler, and P. Hauff, *Small Animal Imaging*, Springer, Berlin, Heidelberg (2011).
2. H. Benveniste and S. Blackband, "MR microscopy and high resolution small animal MRI: applications in neuroscience research," *Prog. Neurobiol.* **67**(5), 393–420 (2002).
3. C. M. Deroose et al., "Multimodality imaging of tumor xenografts and metastases in mice with combined small-animal PET, small-animal CT, and bioluminescence imaging," *J. Nucl. Med.* **48**(2), 295–303 (2007).
4. D. W. Holdsworth and M. M. Thornton, "Micro-CT in small animal and specimen imaging," *Trends Biotechnol.* **20**(8), S34–S39 (2002).
5. D. J. Brenner and E. J. Hall, "Computed tomography—an increasing source of radiation exposure," *N. Engl. J. Med.* **357**(22), 2277–2284 (2007).
6. R. Fazel et al., "Exposure to low-dose ionizing radiation from medical imaging procedures," *N. Engl. J. Med.* **361**(9), 849–857 (2009).
7. G. Brix et al., "Radiation exposure of patients undergoing whole-body dual-modality 18F-FDG PET/CT examinations," *J. Nucl. Med.* **46**(4), 608–613 (2005).
8. L. V. Wang and J. Yao, "A practical guide to photoacoustic tomography in the life sciences," *Nat. Met.* **13**(8), 627–638 (2016).
9. J. Yao et al., "High-speed label-free functional photoacoustic microscopy of mouse brain in action," *Nat. Methods* **12**(5), 407–410 (2015).
10. L. Li et al., "Label-free photoacoustic tomography of whole mouse brain structures ex vivo," *Neurophotonics* **3**(3), 035001 (2016).
11. H.-P. Brecht et al., "Whole-body three-dimensional optoacoustic tomography system for small animals," *J. Biomed. Opt.* **14**(6), 064007 (2009).
12. A. Buehler et al., "Video rate optoacoustic tomography of mouse kidney perfusion," *Opt. Lett.* **35**(14), 2475–2477 (2010).
13. D. Razansky, A. Buehler, and V. Ntziachristos, "Volumetric real-time multispectral optoacoustic tomography of biomarkers," *Nat. Protoc.* **6**(8), 1121–1129 (2011).
14. J. Xia et al., "Whole-body ring-shaped confocal photoacoustic computed tomography of small animals in vivo," *J. Biomed. Opt.* **17**(5), 050506 (2012).
15. J. Yao et al., "Multiscale photoacoustic tomography using reversibly switchable bacterial phytochrome as a near-infrared photochromic probe," *Nat. Methods* **13**(1), 67 (2016).
16. T. T. W. Wong et al., "Use of a single xenon flash lamp for photoacoustic computed tomography of multiple-centimeter-thick biological tissue ex vivo and a whole mouse body in vivo," *J. Biomed. Opt.* **22**(4), 041003 (2017).
17. G. Li et al., "Multiview Hilbert transformation for full-view photoacoustic computed tomography using a linear array," *J. Biomed. Opt.* **20**(6), 066010 (2015).

18. R. Kruger et al., "HYPR-spectral photoacoustic CT for preclinical imaging," *Proc. SPIE* **7177**, 71770F (2009).
19. C. G. Jiang et al., "Immunosuppression in mice induced by cold water stress," *Brain Behav. Immun.* **4**(4), 278–291 (1990).
20. H. Arakawa et al., "Stress increases plasma enzyme activity in rats: differential effects of adrenergic and cholinergic blockades," *J. Pharmacol. Exp. Ther.* **280**(3), 1296–1303 (1997).
21. E. P. Wilder-Smith and A. Chow, "Water-immersion wrinkling is due to vasoconstriction," *Muscle Nerve* **27**(3), 307–311 (2003).
22. ANSftSUoL, *American National Standard for the Safe Use of Lasers*, ANSIZ136, American National Standards Institute, New York (2007).
23. R. Ogura et al., "Specific findings of the standard 12-Lead ECG in patients with 'Takotsubo' cardiomyopathy-comparison with the findings of acute anterior myocardial infarction," *Circ. J.* **67**(8), 687–690 (2003).
24. X. H. Wehrens, S. Kirchhoff, and P. A. Doevendans, "Mouse electrocardiography," *Cardiovasc. Res.* **45**(1), 231–237 (2000).

**Chenghung Yeh** received his BS degree in physics from the National Taiwan University, Taiwan. He is currently a PhD student at Washington University in St. Louis, Missouri, USA. His research interests focus on the application of photoacoustic microscopy (PAM) in biological and medical study.

**Lei Li** received his BS and MS degrees from Harbin Institute of Technology, China, in 2010 and 2012, respectively. He is working as a graduate research assistant under the tutelage of Dr. Lihong Wang at Washington University. His current research focuses on PAM and tomography, especially improving the photoacoustic imaging speed and applying it on brain functional and structural imaging.

**Liren Zhu** is currently a graduate student in biomedical engineering at Washington University in St. Louis under the supervision of Lihong V. Wang, Gene K. Beare distinguished professor. His research focuses on the development of optical imaging, photoacoustic imaging, and ultrasonic imaging techniques for biomedical research.

**Jun Xia** earned his PhD at the University of Toronto and is currently a postdoctoral fellow at Washington University in St. Louis under the mentorship of Dr. Lihong V. Wang. His research interests are the development of biomedical imaging techniques including photoacoustic, photothermal, and ultrasonic imaging. He has published more than 20 peer-reviewed journal articles in photoacoustic and photothermal research.

**Chiye Li** received his BS degree in life sciences from the University of Science and Technology of China in Hefei, China, in 2007. Currently, he is a PhD student in biomedical engineering at Washington University in St. Louis. His research interests involve the application of photoacoustic imaging techniques in biological and medical studies.

**Wanyi Chen** is currently an undergraduate student at Washington University in St. Louis and a research assistant in Dr. Lihong V. Wang's lab. Her research interests are in photoacoustic and ultrasonic imaging.

**Alejandro Garcia-Uribe** received his MSc degree and PhD in electrical engineering from the Department of Electrical and Computer Engineering, Texas A&M University, College Station, Texas. He is currently a research scientist at the Optical Imaging Laboratory, Department of Biomedical Engineering, Washington University in St. Louis. His research interests include biomedical optics, biomedical image analysis, microsensors, and digital signal processing.

**Konstantin I. Maslov** graduated from Moscow Institute of Physics and Technology with a major in biophysics and received his PhD in physical acoustics from Moscow State University, Russia. After graduation, he worked at the Institute of Chemical Physics, Russian Academy of Sciences and Texas A&M University. Currently, he is a research associate professor at the Biomedical Engineering Department, Washington University in St Louis, Missouri. His area of interest includes optical, PA and acoustic imaging, and PA spectroscopy.

**Lihong V. Wang** earned his PhD degree at Rice University, Houston, Texas. He currently holds the Gene K. Beare distinguished professorship of Biomedical Engineering at Washington University in St. Louis. He has published 342 peer-reviewed journal articles and delivered 370 keynote, plenary, or invited talks. His Google Scholar h-index and citations have reached 81 and over 26,000, respectively.